remote sensing

MDPI

Article

Mapping Canopy Base Height Through Integration of GEDI and Sentinel-2 Data

Licheng Zhao [1,2], Wei Guo [3,*] and Cuicui Ji [4]

[1] International Research Center of Big Data for Sustainable Development Goals, Beijing 100094, China
[2] Aerospace Information Research Institute, Chinese Academy of Sciences, Beijing 100094, China
[3] Graduate School of Agricultural and Life Science, The University of Tokyo, Tokyo 188-0002, Japan
[4] School of Smart City, Chongqing Jiaotong University, Chongqing 400074, China
* Correspondence: guowei@g.ecc.u-tokyo.ac.jp

Highlights

What are the main findings?

- The full relative height (RH) profile of GEDI waveform LiDAR can directly identify canopy base height (CBH) as a vertical structural transition, avoiding the need for empirical percentile calibration.
- Integrating sparse GEDI-derived CBH samples with Sentinel-2 optical data (especially SWIR bands and vegetation indices) via machine learning enables highly accurate regional-scale wall-to-wall CBH mapping.

What are the implications of the main findings?

- This physically interpretable framework advances the use of spaceborne LiDAR, showing that complex forest structural boundaries can be detected directly from waveform energy distributions without requiring region-specific airborne LiDAR calibration of the GEDI-based CBH retrieval or empirical allometric equations.
- The methodology provides a scalable and cost-effective approach to mapping continuous forest vertical structures, supplying essential, hard-to-measure parameters for large-scale fire behavior modeling and precision forestry management.

Abstract

Canopy base height (CBH) is a key descriptor of forest vertical structure and an essential input for fire behavior modeling and ecosystem assessments, yet it remains difficult to retrieve reliably from satellite observations. Spaceborne waveform LiDAR from the Global Ecosystem Dynamics Investigation (GEDI) mission provides detailed information on vertical vegetation structure through relative height (RH) metrics, but existing CBH studies have largely relied on empirically selected percentiles or indirect calibration approaches. Here, we present a physically informed framework for CBH estimation that interprets the full GEDI RH profile as a continuous representation of vertical energy distribution and identifies CBH as a structural transition within this profile. Three RH-based approaches—the first-derivative, clustering-threshold, and crown-length methods—were evaluated against independent UAV LiDAR observations. Among them, the clustering-threshold approach achieved the best agreement with UAV-derived CBH (R^2 = 0.71, RMSE = 1.27 m) and was selected for regional-scale mapping. Sparse GEDI-derived CBH samples were further integrated with Sentinel-2 optical data using a gradient boosting regression model to generate wall-to-wall CBH maps for the Jiagedaqi District, northeastern China, achieving an RMSE of 1.01 m against independent validation data. The results demonstrate that CBH can be retrieved directly from GEDI RH metrics without requiring region-specific airborne LiDAR

Check for updates

Academic Editor: Eric Casella

Received: 13 May 2026
Revised: 23 June 2026
Accepted: 25 June 2026
Published: 27 June 2026

Copyright: © 2026 by the authors. Licensee MDPI, Basel, Switzerland. This article is an open access article distributed under the terms and conditions of the Creative Commons Attribution (CC BY) license.

calibration of the GEDI-based CBH retrieval itself, while UAV LiDAR is used only for independent validation. By advancing the interpretation of spaceborne waveform LiDAR for structural boundary detection, this study expands the utility of GEDI data for large-scale mapping of fire-relevant forest structural attributes.

Keywords: canopy base height (CBH); GEDI; waveform LiDAR; Sentinel-2; data fusion; machine learning; forest canopy structure; canopy fuel

1. Introduction

Canopy base height (CBH), defined as the vertical distance between the ground surface and the lowest continuous layer of live canopy foliage, is a fundamental descriptor of forest vertical structure [1–3]. It plays a critical role in regulating forest microclimate, understory light availability, and fuel continuity and serves as an essential input for fire behavior modeling, ecosystem process simulations, and forest management planning [4–6]. Despite its ecological and operational importance, CBH remains one of the most challenging forest structural parameters to retrieve reliably from remote sensing observations [1].

The difficulty in remotely sensing CBH primarily arises from the complex vertical overlap between tree crowns and understory vegetation [2]. In many forest types, particularly those with dense or multi-layered canopies, the transition from ground and understory to the lower canopy does not correspond to a distinct geometric surface but instead reflects a gradual change in vegetation density. Consequently, CBH represents a fuzzy structural boundary rather than a sharply defined height interface, posing a fundamental challenge for remote sensing approaches that rely on discrete height metrics.

Conventional remote sensing techniques face inherent limitations in resolving this structural boundary. Optical satellite data are effective for characterizing horizontal vegetation patterns and canopy cover, yet lack direct sensitivity to the vertical distribution of vegetation elements and often saturate in dense canopies, leading to large uncertainties in CBH estimation [7–9]. Airborne LiDAR provides detailed three-dimensional measurements and has demonstrated strong capability in retrieving CBH [10–13], but its limited spatial coverage, high acquisition costs, and inconsistent temporal availability restrict its suitability for large-scale or repeated monitoring [14]. These constraints motivate the use of spaceborne LiDAR observations, which offer sensitivity to vertical structure combined with broad spatial coverage [15].

The Global Ecosystem Dynamics Investigation (GEDI) mission provides spaceborne waveform LiDAR observations specifically designed to characterize forest vertical structure [16]. GEDI Level 2A products include a set of relative height (RH) metrics that describe the cumulative vertical distribution of returned laser energy within each footprint [17]. While these metrics have been widely applied to estimate canopy height and aboveground biomass [18–22], their application to retrieving canopy structural boundaries such as CBH remains comparatively limited [2]. Most existing approaches rely on a small subset of RH percentiles (e.g., RH50 or RH98), implicitly treating CBH as a discrete height indicator calibrated through regression, which overlooks the continuous nature of waveform energy profiles and has consistently resulted in substantially lower accuracy for CBH than for canopy height or canopy cover in recent large-scale studies [1,23].

In parallel, optical satellite data such as Sentinel-2 provide high spatial resolution and frequent temporal coverage, offering complementary information on canopy cover and horizontal heterogeneity [24,25]. Integrating GEDI waveform LiDAR with optical imagery therefore represents a promising pathway toward spatially continuous CBH mapping. A

key remaining challenge is to develop a fusion framework that preserves the physical interpretability of waveform-derived vertical structure while compensating for the spatial sparsity of GEDI footprints.

In this study, we propose a transferable framework for mapping canopy base height through the integration of GEDI waveform LiDAR and Sentinel-2 data. Rather than relying on predefined RH percentiles, we interpret the full GEDI RH profile as a continuous representation of vertical energy distribution and identify canopy base height as a structural transition embedded within this profile. This physically informed interpretation is combined with machine learning-based feature integration to generate spatially continuous CBH maps without requiring region-specific airborne LiDAR calibration of the GEDI-based CBH retrieval itself. Independent UAV LiDAR data are used solely for validation and threshold sensitivity assessment. Specifically, the objectives of this study are to (1) investigate the capability of the full GEDI RH vertical profile to delineate canopy base height as a structural transition rather than a discrete height metric; (2) develop an integrated GEDI–Sentinel-2 framework for spatially continuous CBH mapping; and (3) evaluate the accuracy and robustness of the proposed method under heterogeneous canopy structural conditions using independent UAV LiDAR observations. By advancing the interpretation of spaceborne waveform LiDAR for forest structural boundary detection, this study enhances the potential of GEDI data for large-scale forest vertical structure monitoring.

2. Materials and Methods

2.1. Experimental Design

The methodology of this study consists of three main components:

(1) Development of a GEDI-based CBH retrieval algorithm—An algorithm was designed to estimate CBH directly from GEDI height metrics data, enabling footprint-scale measurements of CBH.

(2) UAV LiDAR validation—High-resolution unmanned aerial vehicle (UAV) LiDAR data were acquired and processed to derive CBH estimates, which were used to evaluate the accuracy of the GEDI-derived CBH results.

(3) Regional-scale extrapolation—Sparse CBH samples obtained from GEDI were integrated with Sentinel-2 multispectral data, terrain variables, and land cover information as auxiliary predictors in a machine learning framework to generate spatially continuous, regional-scale CBH maps.

The overall workflow is illustrated in Figure 1.

2.2. Study Area

This study was conducted in a representative forested region in northeastern China: the Jiagedaqi District in Heilongjiang Province (Figure 2). Jiagedaqi District (123°45′–124°26′E, 50°09′–50°35′N) is located on the southeastern slope of the Greater Khingan Mountains. Administratively, the district belongs to the Daxing'anling Prefecture of Heilongjiang Province, although its land jurisdiction lies within the Oroqen Autonomous Banner of the Inner Mongolia Autonomous Region. It serves as the political, economic, cultural, and transportation hub of the Greater Khingan region, which is known for its extensive, well-preserved boreal forests and is one of China's most important forestry bases. The district covers an area of 1359 km^2, with 90,207 ha of forest land. Topographically, Jiagedaqi lies in the foothills of the Greater Khingan Mountains, characterized by gently undulating low hills, with higher elevations in the northwest and lower elevations in the southeast. Low hills surround the urban area, while flatlands are mainly distributed along the north and south banks of the Ganhe River. The average elevation is 472 m, and the area experiences a cold temperate continental monsoon climate. Vegetation belongs to the

cold-temperate coniferous forest zone of the Greater Khingan mountain belt, forming the southern extension of the Siberian mountain coniferous forests. The flora is dominated by the Daurian floristic region, with minor elements from the Changbai and Inner Mongolian floras. Major tree species include *Larix gmelinii* (Dahurian larch), *Pinus sylvestris* var. *mongolica* (Scots pine), *Betula* spp. (birch), *Populus davidiana* (aspens), *Salix* spp. (willow), *Quercus mongolica* (Mongolian oak), and *Picea koraiensis* (Korean spruce), with birch accounting for the largest timber volume. Jiagedaqi is renowned as one of China's most important forest regions.

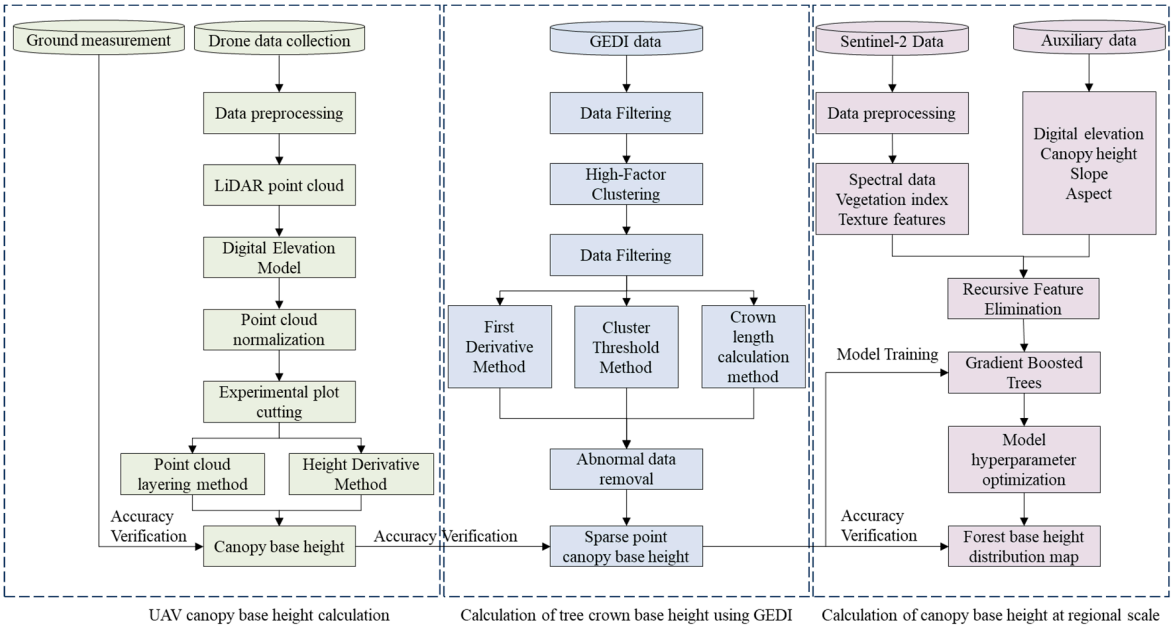


Figure 1. Workflow for canopy base height estimation.

2.3. Data Collection

2.3.1. GEDI

The GEDI instrument was launched on 5 December 2018 and is mounted aboard the International Space Station (ISS). GEDI is designed to characterize ecosystem structure and dynamics, thereby fundamentally improving the quantification and understanding of the global carbon cycle and biodiversity. The instrument acquires high-resolution laser ranging observations of the Earth's three-dimensional structure.

Since April 2019, NASA's GEDI spaceborne lidar has been providing footprint-level measurements of vegetation structure, including forest canopy height, between 51.6°N and 51.6°S globally. GEDI achieves the highest spatial resolution and densest sampling of any spaceborne light detection and ranging (LiDAR) instrument to date. The instrument comprises three lasers generating eight ground tracks, each with an average footprint diameter of approximately 25 m and along-track spacing of ~60 m. Across-track beam spacing is ~600 m, resulting in a swath width of ~4.2 km.

GEDI's measurements of forest canopy height, vertical canopy structure, and ground elevation greatly enhance our capacity to characterize carbon and water cycle processes, biodiversity, and habitat quality. Additionally, GEDI data have significant applications in weather forecasting, forest management, snow and glacier monitoring, and the generation of digital elevation models.

This study utilized GEDI's Level 2A Geolocated Elevation and Height Metrics product (GEDI02_A), distributed by NASA's Land Processes Distributed Active Archive Center (LP DAAC; Sioux Falls, SD, USA), which contains 101 RH metrics describing the vertical distribution of waveform energy. The original GEDI02_A product is provided as a footprint-

level point dataset with a nominal spatial resolution (mean footprint diameter) of 25 m. For our analysis, monthly raster composites of GEDI L2A data were obtained from the Google Earth Engine (GEE) platform.

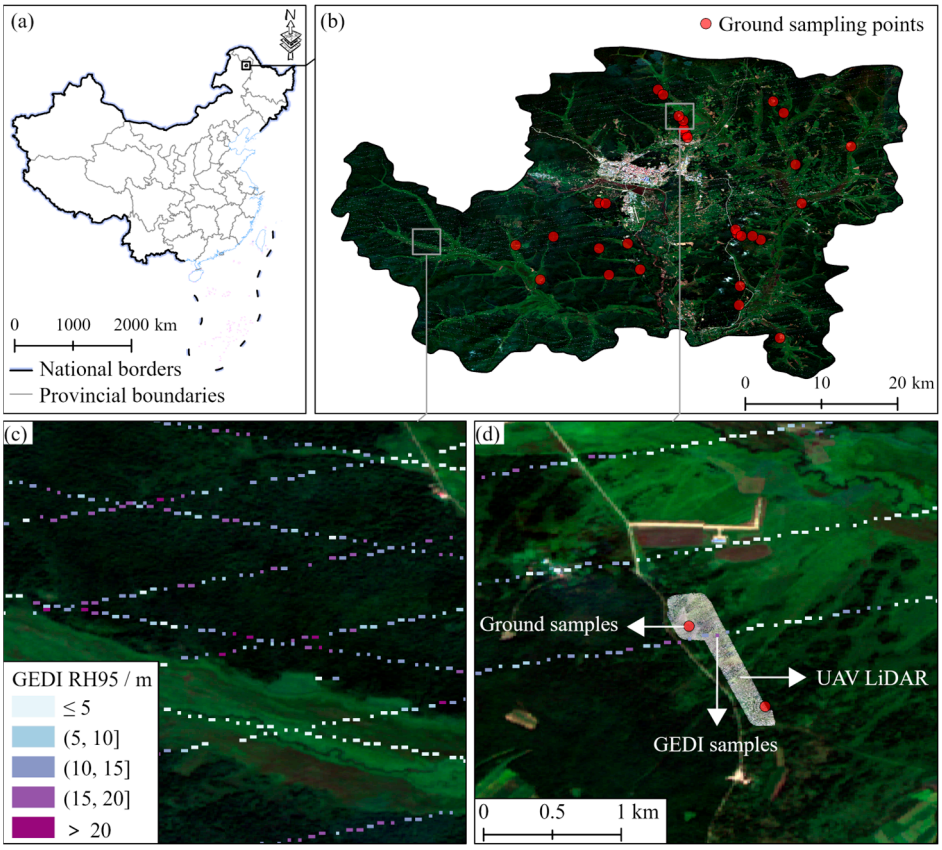


Figure 2. Study area. (**a**) Location of the study area within China; (**b**) Sentinel-2 image of the study area overlaid with GEDI footprints, UAV coverage, and ground sampling points, where red dots denote the ground sampling plots; (**c**,**d**) enlarged views of the highlighted subregions, with (**d**) illustrating the overlap of the UAV LiDAR coverage with the GEDI footprints and ground samples within the enlarged area.

2.3.2. UAV LiDAR

ALS data for the Jiagedaqi area were acquired using a DJI Matrice 300 RTK UAV (SZ DJI Technology Co., Ltd., Shenzhen, China) equipped with an advanced Zenmuse L1 LiDAR sensor (SZ DJI Technology Co., Ltd., Shenzhen, China). The M300 RTK offers exceptional stability and maneuverability, enabling safe and efficient operation under complex terrain and meteorological conditions. The wavelength characteristics of the L1 sensor make it well-suited for capturing detailed vegetation structural information. The high spatial resolution and accuracy of the collected LiDAR data provided a reliable basis for calculating CBH at the plot scale.

Flight altitude was adjusted according to local topographic conditions, ranging from 50 to 300 m above ground level. Flight planning parameters included a forward overlap of 70% and a side overlap of 60%, with the LiDAR configured to record up to three returns per pulse. Each individual flight lasted approximately 30 min. The Zenmuse L1 sensor produces high-density point clouds suitable for detailed canopy structure analysis. In our flights, the average point density ranged between 152.29– and 4062.89 points per m^2, depending on flight altitude and terrain (Figure 3). This density exceeds the minimum required for trunk–crown transition detection reported in previous studies [12,13] and provides stable layer-wise statistics for implementing the stratification method. The acquired UAV LiDAR

data were preprocessed using DJI Terra software (v3.6.0; SZ DJI Technology Co., Ltd., Shenzhen, China) to produce classified point cloud data in LAS format for subsequent CBH computation.

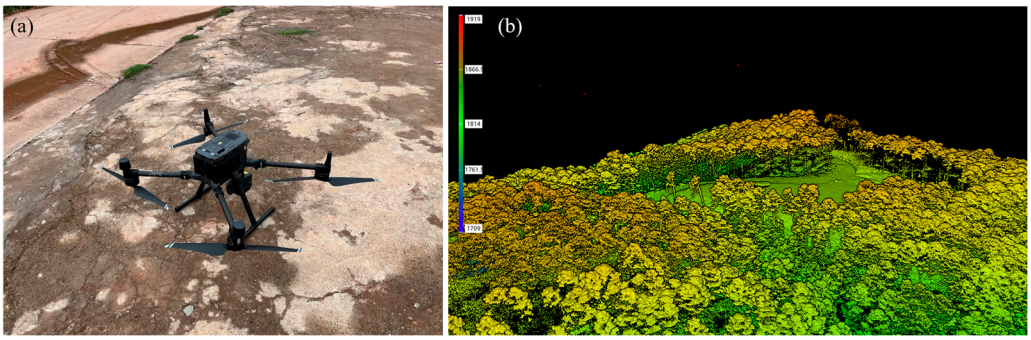


Figure 3. UAV LiDAR system and sample data used in this study. (**a**) UAV systems used in this study; (**b**) UAV lidar data collected.

2.3.3. Sentinel-2 Data

The Sentinel-2 constellation, operated by the European Space Agency (ESA), consists of two identical satellites—Sentinel-2A and Sentinel-2B—each carrying a MultiSpectral Instrument (MSI). Operating at an altitude of 786 km, the MSI acquires imagery across 13 spectral bands with spatial resolutions of 10 m, 20 m, and 60 m and a swath width of 290 km. Sentinel-2A has a revisit cycle of 10 days, which is reduced to 5 days when combined with Sentinel-2B.

The spectral range of Sentinel-2 spans from the visible and near-infrared (VNIR) to the shortwave infrared (SWIR) regions. Notably, the MSI includes three red-edge bands, which are particularly effective for monitoring vegetation health and canopy characteristics.

In this study, Sentinel-2 spectral reflectance data, together with derived vegetation indices (e.g., NDVI), texture metrics, and the annual maximum NDVI, were used as predictor variables in the CBH extrapolation model.

2.3.4. Field Survey

A field survey was conducted in August 2022 in the Jiagedaqi District of the Greater Khingan Mountains, Heilongjiang Province, China. In the field, CBH was defined as the vertical distance from the ground to the lowest live branches forming part of the main crown (Figure S1). Small, isolated leafy branches separated from the main crown were not considered indicative of CBH. Measurements were recorded using a laser hypsometer.

To minimize potential errors from mixed pixels in remote sensing data, sampling plots were located in homogeneous forest stands situated away from water bodies, roads, and buildings. Each plot was established using either two 30 m transects intersecting at 90°, or three 30 m transects intersecting at 60°, with the plot center coordinates recorded using a Trimble Juno 3B handheld GPS receiver (Trimble Inc., Sunnyvale, CA, USA). Within each plot, 15–30 representative trees were selected for CBH measurement, and the plot-level CBH value was calculated as the mean of these measurements.

A total of 18 plots were surveyed, covering dominant tree species including *Pinus sylvestris*, *Larix gmelinii* (larch), *Betula* spp. (birch), *Quercus mongolica* (oak), and *Populus* spp.

2.3.5. Auxiliary Data

To enable regional-scale CBH mapping, additional auxiliary datasets were incorporated alongside Sentinel-2 imagery. These included land cover data, forest canopy height data, and topographic variables.

Land cover data were obtained from the GLC_FCS30D dataset [26], which provides global land cover maps at 30 m spatial resolution from 1985 to 2022. The dataset adopts a detailed classification scheme with 35 land cover classes, in which forest is subdivided into 10 categories based on canopy closure (open/closed), phenology (evergreen/deciduous), leaf type (broadleaved/needle-leaved), and mixed forest types. Land cover data corresponding to the inversion year were used as predictor variables in the CBH extrapolation model.

Forest canopy height data were sourced from a newly developed global 30 m resolution canopy height product, generated through the integration of GEDI lidar forest structure measurements and Landsat analysis-ready time-series data [18].

Topographic data were obtained from NASA's Shuttle Radar Topography Mission (SRTM) 30 m digital elevation model (DEM), which provides near-global coverage [27]. From the DEM, slope and aspect were derived based on the rate of elevation change in the north–south and east–west directions, calculated as

$$S = \arctan\sqrt{f_x^2 + f_y^2} \quad (1)$$

$$A = 270^\circ + \arctan(f_y/f_x) - 90^\circ f_y/|f_x| \quad (2)$$

where S and A represent slope and aspect, respectively, and f_x and f_y denote the elevation change rate in the north–south and east–west directions.

2.4. Estimation of Footprint-Scale CBH from Spaceborne LiDAR Data

To ensure reliable detection of the canopy–trunk transition, we used the complete sequence of 101 RH metrics (RH0–RH100) provided by the GEDI L2A product. CBH corresponds to the height at which the waveform energy shifts from the low-density trunk region to the high-density crown region. The location of this transition varies substantially across species, stand densities, age classes, and vertical fuel structures and therefore does not necessarily align with fixed RH percentiles such as RH10, RH25, or RH50. Using only a reduced subset would not preserve the full shape of the vertical energy profile and would prevent accurate detection of inflection points or density thresholds. The full RH sequence has been shown in previous studies to better represent vertical canopy structural diversity [22,23]. For these reasons, the complete RH vector was retained to ensure consistency, generality, and robustness across different forest types. To ensure structural stability and deliberately avoid the severe waveform degradation caused by leaf-off conditions in deciduous and mixed stands, a strict temporal filter was applied to the spaceborne observations. For the Jiagedaqi District, all available GEDI footprints were extracted exclusively during the peak growing season (i.e., strict leaf-on conditions) between July and September 2022. Following this temporal selection, quality control procedures were applied to retain only the laser returns meeting waveform integrity criteria—based on energy, sensitivity, amplitude, and real-time surface tracking quality—as well as valid pointing and geolocation status.

2.4.1. GEDI Point Filtering Using Clustering Algorithms

To separate canopy and ground returns, GEDI RH metrics were subjected to clustering analysis using three algorithms: K-Means, Mean Shift, and DBSCAN.

(1) K-Means is an iterative partitioning algorithm that groups data points into KKK user-defined clusters by minimizing the sum of squared distances between points and their respective cluster centroids. While widely used, K-Means is sensitive to the shape and size of clusters.

(2) Mean Shift is a density-based clustering method that does not require prior specification of the number of clusters. It iteratively shifts each data point toward the region of highest density in feature space, making it robust to irregularly shaped clusters and noise. This method is commonly applied in image segmentation and object tracking.
(3) DBSCAN (Density-Based Spatial Clustering of Applications with Noise) is another density-based method that identifies clusters as areas of high point density separated by areas of low density. It requires no prior specification of the number of clusters and is effective for datasets with varying cluster shapes and sizes, as well as noisy data.

A subset of GEDI footprints was randomly sampled to evaluate the three clustering algorithms. Among them, Mean Shift demonstrated the most reliable performance in separating canopy and ground returns across forested environments. To refine the parameterization, the bandwidth-related quantile parameter was optimized through empirical testing. We assessed values between 0.2 and 0.6 by comparing the resulting cluster boundaries with the vertical distribution of energy in the corresponding UAV-derived point clouds. A quantile of 0.4 produced the highest consistency between the crown-related cluster and the canopy energy concentration in the high-resolution LiDAR profiles and was therefore selected for all subsequent analyses. The n_samples parameter was fixed at 101 to match the dimensionality of the GEDI RH vector (RH0–RH100), reflecting a structural property of the input data rather than a tunable hyperparameter.

Mean Shift was ultimately chosen over K-Means and DBSCAN due to its conceptual and practical advantages for this application. Unlike K-Means, Mean Shift does not assume spherical clusters or require predefining the number of clusters, and unlike DBSCAN, it is less sensitive to parameter choices in a one-dimensional feature space. Most importantly, Mean Shift consistently identified the two dominant density modes representing ground and crown energy peaks, enabling robust vertical segmentation of GEDI RH profiles.

Based on the clustering results, each GEDI footprint's height metrics were classified into two groups—canopy and ground. Only footprints with exactly two identified classes, where the minimum cluster centroid ranged between -1 and 1 m, were retained. For footprints where only one class was detected and the cluster centroid fell within -1 m $< X <$ 1 m, CBH was directly set to zero. This filtering step ensured that only footprints representing a clear two-layer vertical structure (canopy and ground) were retained, while excluding footprints containing multiple vegetation strata. This strict filtering ensured the high purity of training data required for regional extrapolation. The capability of this framework to process multi-layered canopies using an adaptive multi-cluster algorithm is further evaluated in Section 4.5.

For each retained footprint, CBH was then calculated using three independent methods: (1) the first derivative method; (2) the clustering threshold method; and (3) the crown length method.

2.4.2. First Derivative Method

The first derivative method is based on the principle that vegetation density is lower in the trunk region and higher in the crown region. For equal vertical height intervals, spaceborne LiDAR returns from the trunk contain less energy, whereas those from the crown contain more. Inflection points in the waveform correspond to local maxima or minima in the fitted function, occurring when the first derivative (slope) reaches a local extreme and the second derivative equals zero [28]. Thus, by differentiating the GEDI height–energy profile, the height at which a sharp increase in energy occurs is interpreted as the transition from trunk to crown, corresponding to CBH (Figure 4f).

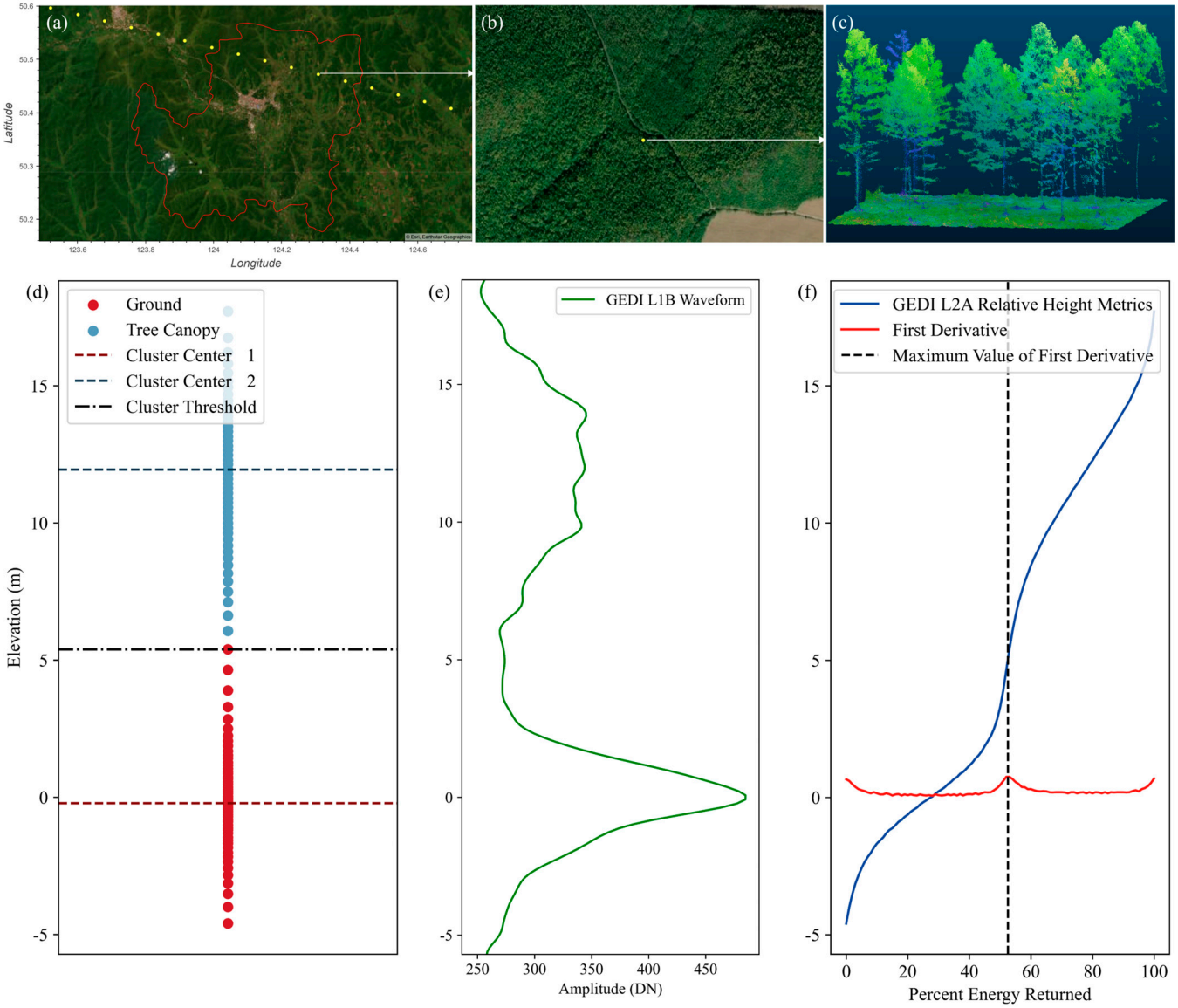


Figure 4. Methods for CBH estimation from GEDI footprints. (**a**) A representative GEDI ground track; (**b**) individual GEDI footprint locations; (**c**) forest stand corresponding to a GEDI footprint; (**d**) vertical distribution of GEDI L2A relative height (RH) metrics for the footprint shown in (**b**), together with the Mean Shift clustering results; (**e**) corresponding GEDI L1B geolocated waveform for the footprint shown in (**b**); (**f**) height profile of GEDI L2A percent energy returned and its first derivative, with the detected trunk–crown transition indicated.

2.4.3. Clustering Threshold Method

This method assumes that the primary energy sources of tree returns originate from the crown and the ground. By vertically clustering GEDI height metrics, two groups are identified: ground returns and crown returns (Figure 4d). The boundary separating these clusters represents the local density minimum between the two energy modes. While this statistical threshold provides a robust demarcation between ground and canopy energy structures, it fundamentally represents an intermediate transitional position rather than the exact physical location of the lowest continuous live foliage. However, because understory vegetation is typically aggregated into the ground cluster, this statistical boundary serves as a robust and scalable proxy for the CBH position in spaceborne LiDAR observations.

2.4.4. Crown Length Method

The crown length method estimates CBH as the difference between tree height and crown length. The canopy cluster centroid obtained from vertical clustering is used to approximate the crown center height, while tree height is derived from the RH95 metric (Figure 4d). CBH is calculated based on the geometric assumption of a vertically symmetrical crown. Under this idealization, the crown center (CC) is assumed to be positioned exactly midway between the canopy base and the tree top. The relationship is expressed as

$$CBH = CH - 2 \times (CH - CC) \tag{3}$$

which mathematically simplifies to

$$CBH = 2 \times CC - CH \tag{4}$$

where CBH is the canopy base height, CH is the canopy height (derived from the RH95 metric), and CC is the canopy center height (approximated by the canopy cluster centroid). It must be acknowledged that this is a simplifying assumption, as natural tree crowns are rarely perfectly symmetrical in the vertical profile.

2.5. CBH Estimation from UAV LiDAR Data

UAV LiDAR data were processed using DJI Terra software for point cloud reconstruction. Laser returns beyond 250 m from the LiDAR sensor were excluded, and the resulting point cloud dataset for the study area was generated (Figure 5a). The point cloud was classified in ENVI LiDAR (v5.6; NV5 Geospatial, Broomfield, CO, USA) to separate ground returns, which were then used to generate a DEM. The DEM was subsequently used in Python (v3.9; Python Software Foundation, Wilmington, DE, USA) to normalize the original point cloud, producing terrain-corrected point cloud data for the study area (Figure 5b).

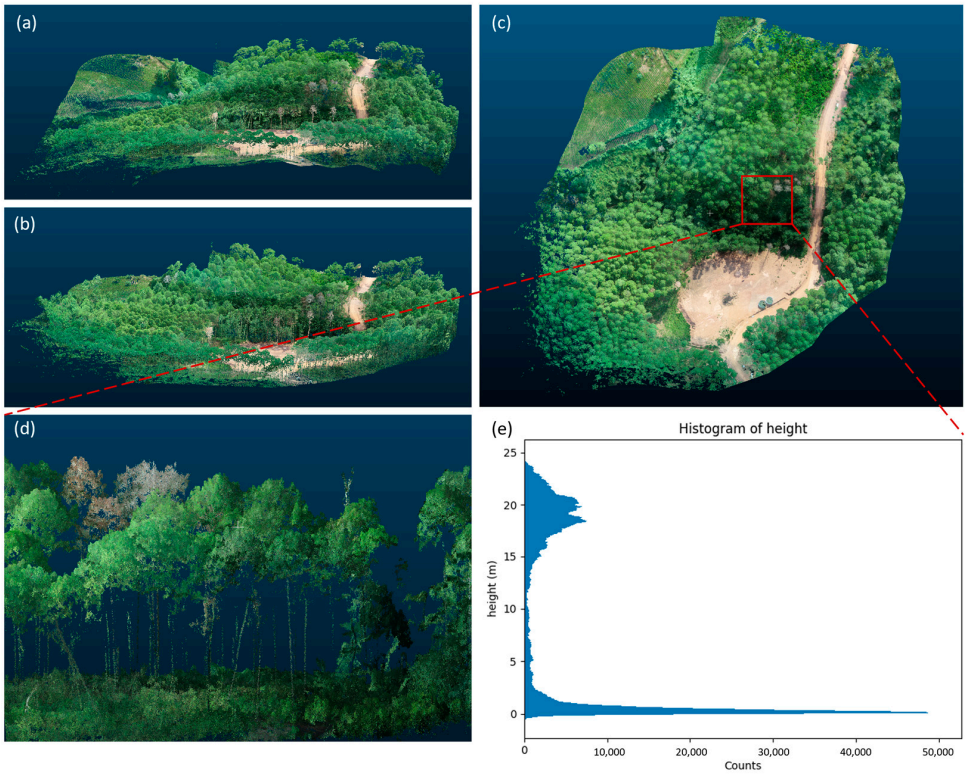


Figure 5. Workflow for UAV LiDAR data processing. (**a**) Raw UAV LiDAR point cloud. (**b**) Normalized point cloud. (**c**) Preprocessed point cloud. (**d**) Clipped point cloud. (**e**) Point cloud counts by height layers.

The calculation areas were delineated in ArcGIS (v10.8; Esri, Redlands, CA, USA) and saved as Shapefile format (Figure 5c). Using Python, the terrain-corrected point cloud was clipped to these areas of interest, and the resulting subsets were used for CBH estimation (Figure 5d). CBH was calculated from the preprocessed point cloud using two algorithms (Figure 6):

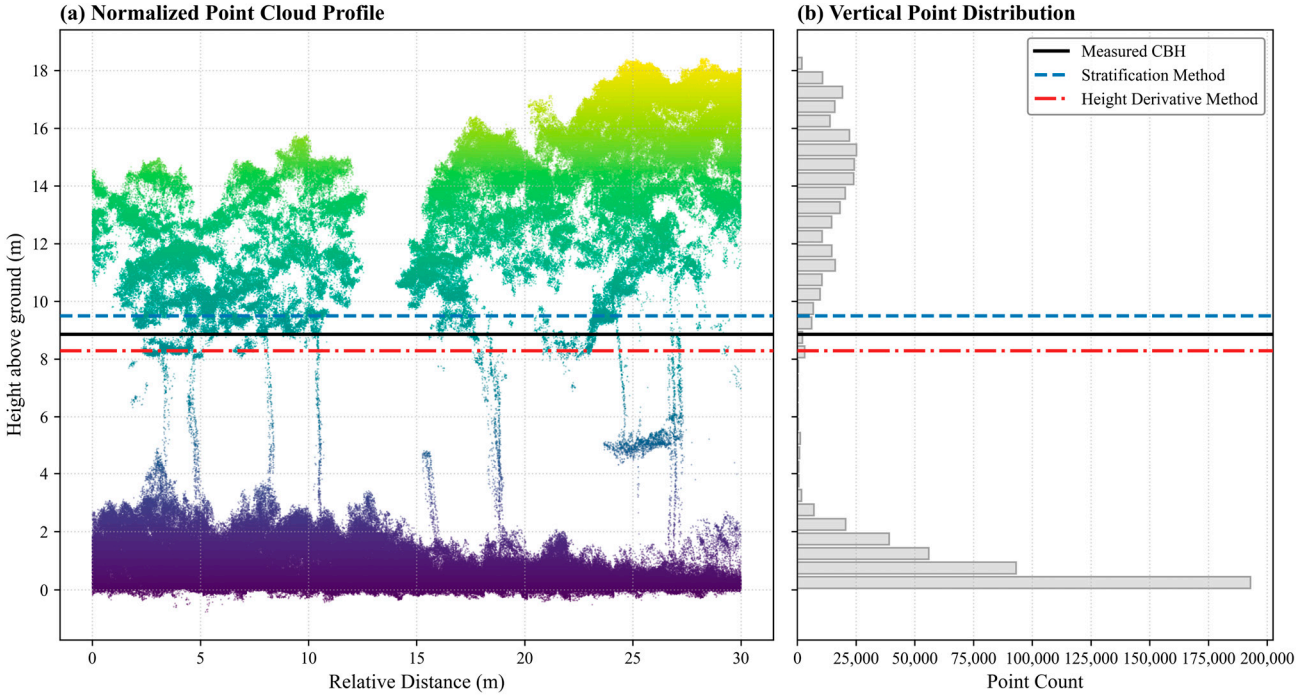


Figure 6. Demonstration of CBH estimation using two LiDAR-based algorithms on a sample tree. (**a**) Side view of the terrain-corrected point cloud. (**b**) Vertical height profile illustrating point counts at 0.5 m intervals. The black solid line represents the ground-measured CBH. The dashed red line and dot-dashed blue line indicate the CBH calculated by the Point Cloud Stratification Method and the Point Cloud Height Derivative Method, respectively.

2.5.1. Point Cloud Stratification Method

This method is based on the assumption that vegetation density varies vertically within the forest profile—being higher in the crown region and lower in the trunk region. The transition from sparse to dense point distribution indicates the CBH position.

In this approach, the normalized point cloud was stratified at 0.5 m vertical intervals. The number of points in each layer was calculated and compared with 1% of the total number of points above 2 m. Layers with fewer points than this threshold were assigned a value of 0, and those exceeding the threshold were assigned a value of 1. The CBH position was defined as the first height where the value transitioned from 0 to 1.

The 1% threshold was rigorously determined through a sensitivity analysis that compared UAV-estimated CBH against ground measurements across a range of stratification thresholds from 0.5% to 3.0% (Figure S2). As illustrated in the supplementary analysis, the 1.0% threshold is an optimized structural boundary that yields the highest agreement with field data, achieving the minimum Root Mean Square Error (RMSE = 1.35 m) and Mean Absolute Error (MAE = 0.99 m), alongside the highest Coefficient of Determination (R^2 = 0.69).

Deviating from this optimum compromises the detection accuracy: lower thresholds (e.g., 0.5%) amplify the algorithm's sensitivity to understory noise and isolated branches, causing severe underestimations, while higher thresholds (1.5% to 3.0%) systematically overestimate CBH by neglecting the sparse foliage at the lower canopy limit. Therefore,

rather than being an empirical approximation, the 1% criterion represents a robust, physically optimized balance between noise suppression and transition detection, ensuring the reliability of the UAV-derived ground truth across heterogeneous stands.

2.5.2. Point Cloud Height Derivative Method

This method relies on the observation that the rate of change in height between consecutive percentiles of the point cloud distribution differs between the trunk and crown regions. Specifically, the height difference between equal percentile intervals is greater in the trunk region than in the crown region.

In this approach, the height values corresponding to every 5th percentile of the point cloud distribution were computed, and the first derivative was calculated. The CBH position was identified as the height corresponding to the maximum first derivative, representing the point of greatest height increase, consistent with the principle that extrema of the derivative of a fitted vertical profile mark structural transition point [28].

2.6. Wall-to-Wall Mapping of CBH Using GEDI and Sentinel-2 Data

The CBH retrieval method based on GEDI spaceborne LiDAR provides sparse-footprint measurements within the study area. To produce a spatially continuous CBH distribution (wall-to-wall mapping), we integrated GEDI-derived CBH samples with Sentinel-2 optical imagery, forest canopy height products, and terrain data within a machine learning framework.

A gradient boosting tree (GBT) algorithm was employed for regional-scale mapping. GBT is a powerful ensemble learning method widely used for both regression and classification tasks. It builds a strong predictive model by sequentially adding decision trees, with each new tree trained to fit the residual errors of the combined model from previous iterations. The process involves initializing the model, computing residuals, fitting new trees, updating the model, and repeating the procedure until a stopping criterion is met (e.g., maximum iteration number or minimal residual error). Advantages of GBT include robustness to overfitting, the ability to handle heterogeneous features, and high predictive accuracy.

The input features for CBH mapping were categorized into six groups: spectral bands, vegetation indices, texture metrics, topography, forest canopy height, and land cover.

(1) Spectral: 12 Sentinel-2 spectral bands.
(2) Vegetation indices: 17 vegetation indices calculated from Sentinel-2 reflectance data.
(3) Texture features: Nine texture metrics for each of NIR, NDVI, and BI, calculated from the gray-level co-occurrence matrix (GLCM), using a 3×3 moving window.
(4) Topography: Elevation, slope, and aspect.
(5) Land cover: 30 m land cover classification from the GLC_FCS30D product.
(6) Forest canopy height.

Spectral, vegetation index, and texture features were computed as median composites over six 60-day periods in 2022. In addition, the annual maximum NDVI (NDVI_max), forest canopy height [18], and land cover data [26] were included as predictors. The final feature set comprised 342 variables in total (Table 1).

Optical predictor variables were derived from 60-day composite images. This temporal window was chosen to balance data availability and seasonal specificity. In some parts of the study region, frequent cloud cover limits the number of valid optical observations, and a 30-day window may result in insufficient usable pixels or unstable reflectance values. Conversely, extending the interval to 90 days would smooth short-term seasonal differences in vegetation condition and background reflectance, thereby reducing the variability that is informative for CBH-related structural estimation. The 60-day window therefore provides

a practical compromise, ensuring adequate data availability while preserving meaningful seasonal signals. The 3 × 3 GLCM window is widely used in vegetation and forest structural studies because it captures fine-scale heterogeneity while minimizing the smoothing effects associated with larger neighborhoods [29].

Table 1. Predictor variables used for CBH wall-to-wall mapping.

Type	Features
Spectral (60-day median composites)	B1: Coastal/Aerosol; B2: Blue; B3: Green; B4: Red; B5: Red-edge 1; B6: Red-edge 2; B7: Red-edge 3; B8: Near-infrared (NIR); B8A: Narrow NIR; B9: Water vapor; B11: SWIR; B12: SWIR
Vegetation indices (60-day median composites)	$NDVI = \frac{B8-B4}{B8+B4}$ $NDWI = \frac{B3-B8}{B8+B3}$ $NDWI2 = \frac{B8A-B11}{B8A+B11}$ $SAVI = \frac{(B8A-B4)\times(1+0.5)}{(B8A+B4+0.5)}$ $IBI = \frac{\frac{2\times B11}{B11+B8}-\left(\frac{B8}{B8+B4}+\frac{B3}{B3+B11}\right)}{\frac{2\times B11}{B11+B8}+\left(\frac{B8}{B8+B4}+\frac{B3}{B3+B11}\right)}$ $RVI = \frac{B8}{B4}$ $DVI = B8 - B4$ $BI = \sqrt{B2^2 + B3^2 + B4^2}$ $EVI = \frac{2.5\times(B8-B4)}{B8+6\times B4-7.5\times B2+1}$ $MSAVI = \frac{2\times B8+1-\sqrt{(2\times B8+1)^2-8\times(B8-B4)}}{2}$ $RGVI = \frac{B4-B3}{B4+B3}$ $ARVI = \frac{B8-(2\times B4-B2)}{B8+(2\times B4-B2)}$ $VARI = \frac{B3-B4}{B3+B4-B2}$ $GNDVI = \frac{B8-B3}{B8+B3}$ $NS1 = \frac{B8-B11}{B8+B11}$ $NS2 = \frac{B8-B12}{B8+B12}$ $SWSW = \frac{B11-B12}{B11+B12}$
Texture (60-day median composites)	Angular Second Moment (ASM); Contrast; Variance (VAR); Inverse Differential Moment (IDM); Sum Average (SAVG); Sum Variance (SVAR); Sum Entropy (SENT); Entropy (ENT); Dissimilarity (DISS)
Topography	Elevation, slope, aspect
Forest canopy height	Global Forest Canopy Height
Land cover classification	GLC_FCS30-2020

2.7. Accuracy Assessment

The accuracy assessment of CBH estimation was conducted in three steps. First, ground measurements were compared with UAV LiDAR-derived CBH to verify the reliability of the UAV-based estimation algorithms. Second, UAV LiDAR data from areas overlapping with GEDI footprints were used to validate the GEDI-based CBH retrieval method. Finally, the GEDI-derived CBH samples were used to assess the accuracy of the regional-scale (wall-to-wall) CBH mapping results.

Three statistical metrics were used for evaluation: the coefficient of determination (R^2), mean absolute error (MAE), and root mean square error (RMSE), calculated as follows:

$$R^2 = 1 - \frac{\sum(y_i - \hat{y}_i)^2}{\sum(y_i - \overline{y})^2} \quad (5)$$

$$MAE = \frac{1}{n}\sum_{i=1}^{n}|y_i - \hat{y}_i| \quad (6)$$

$$RMSE = \sqrt{\frac{1}{n}\sum_{i=1}^{n}(y_i - \hat{y}_i)^2} \quad (7)$$

where n is the number of sample points, $\hat{y}_i$ is the model-predicted value, y_i is the reference value, and $\bar{y}$ is the mean of the reference values.

3. Results

3.1. Accuracy of UAV-Based CBH Estimation

UAV LiDAR data corresponding to ground sampling plots were clipped and processed using both the point cloud stratification method and the height derivative method to estimate CBH. The results were compared against field measurements (Figure 7).

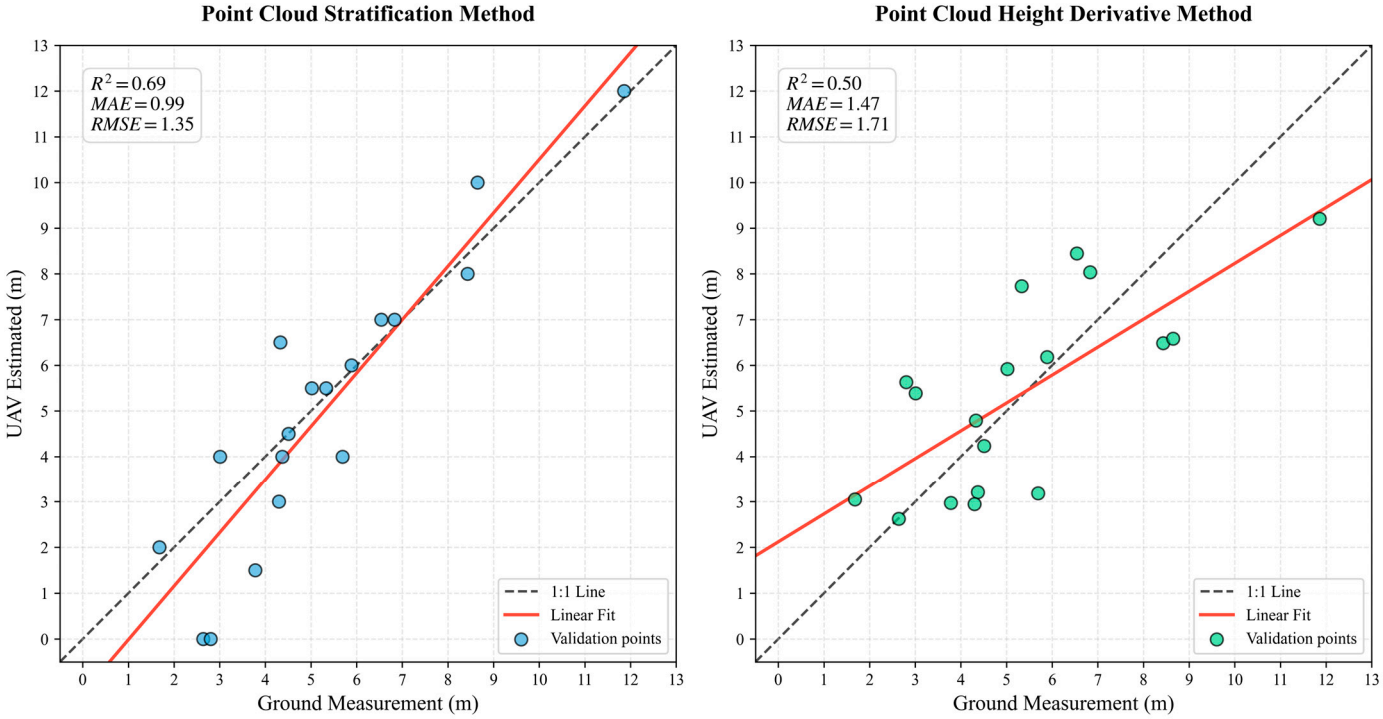


Figure 7. Accuracy assessment of CBH estimation from UAV LiDAR.

For the stratification method, the estimated CBH achieved an R^2 of 0.69, an MAE of 0.99 m, and an RMSE of 1.35 m relative to ground measurements. In comparison, the height derivative method yielded an R^2 of 0.50, an MAE of 1.47 m, and an RMSE of 1.71 m.

The stratification method yielded higher accuracy metrics than the height derivative method and was therefore used for subsequent CBH calculations across the study area.

3.2. Footprint-Scale CBH Estimation from Spaceborne Lidar

UAV-based CBH measurements addressed the issue of spatial discontinuity in field surveys; however, the limited spatial coverage of UAV LiDAR makes it challenging to obtain large-scale datasets. To overcome this limitation, we utilized spaceborne LiDAR data to acquire CBH samples over the study area.

Using three algorithms—the first derivative method, clustering threshold method, and crown length method—we calculated CBH values for GEDI footprints overlapping with UAV LiDAR data and compared them against UAV-derived CBH estimates (Figure 8).

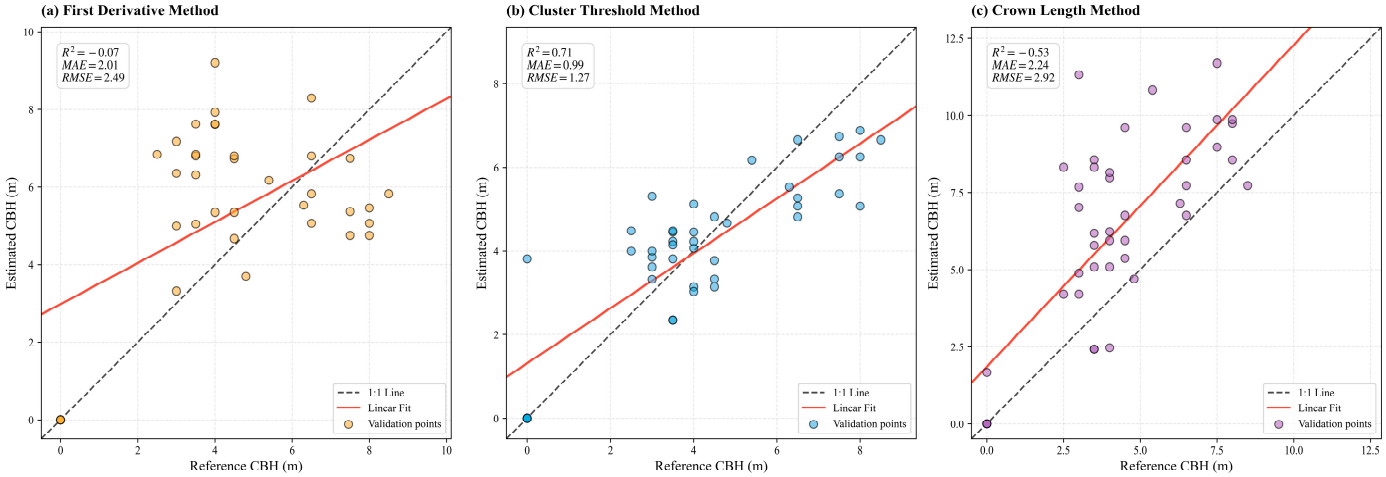


Figure 8. Validation of canopy base height estimation derived from spaceborne LiDAR using the clustering threshold method.

The results show that the clustering threshold method achieved the highest accuracy, with R^2 = 0.71, MAE = 0.99 m, and RMSE = 1.27 m. In contrast, the first derivative method and crown length method yielded lower accuracies. For the first derivative method, estimation errors mainly arose from footprints with low return energy in the ground or canopy layers, leading to incorrect detection of transition points. The crown length method generally followed the overall trend but produced a substantial number of systematically overestimated points. As explicitly noted in Section 2.4.4, this method relies on the simplifying assumption of a vertically symmetrical crown, utilizing the relationship $CBH = 2 \times CC - CH$. In reality, due to light competition, the upper canopy is typically much denser than the lower canopy. This structural asymmetry pulls the actual energy centroid (CC) toward the upper-middle crown region. Consequently, the mathematically inflated CC value directly drives the systematic overestimation of CBH observed in this method.

Based on the comparative analysis, the clustering threshold method was selected for subsequent GEDI-based CBH estimation. Accordingly, CBH samples at the sparse-point scale for the entire study area were generated using GEDI data processed with the clustering threshold method (Figure 9).

3.3. Regional-Scale CBH Estimation Accuracy

Using the clustering threshold method applied to GEDI footprints, we obtained 8207 sparse-point CBH samples for the Jiagedaqi District. These samples were combined with preprocessed remote sensing spectral bands, vegetation indices, texture features, topography, forest height, and land cover data to form a dataset with a total of 342 features. A GBT regression approach was adopted for large-scale CBH extrapolation.

Out of the 8207 total GEDI CBH samples, exactly 6566 samples (80%) were allocated for model training, 821 samples (10%) for hyperparameter tuning, and 820 samples (10%) reserved as a completely independent validation set.

Recursive Feature Elimination (RFE) was performed on the training set to reduce dimensionality and mitigate potential overfitting. In the initial full feature space (342 features), the training-sample-to-feature ratio was approximately 19.2:1. Model performance stabilized at 130 features (comprising 25 spectral features, 44 vegetation indices, 57 texture features, 3 topographic features, and 1 forest height feature). This feature reduction significantly improved the ratio to 50.5 training samples per feature (6566/130).

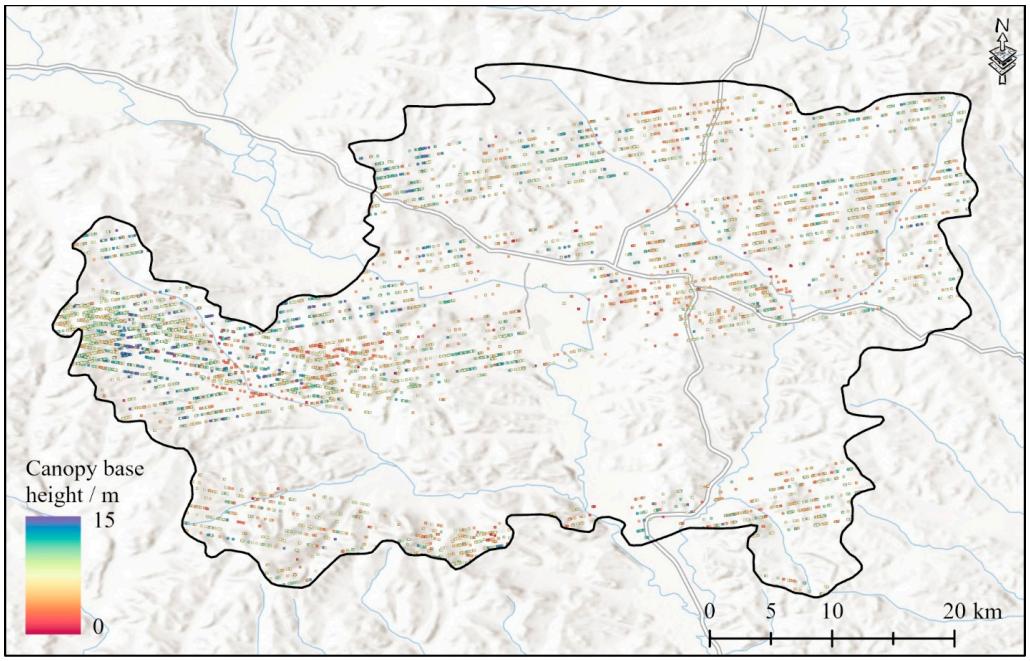


Figure 9. Canopy base height estimation from GEDI using clustering threshold method.

Using these 130 features, hyperparameter tuning on the 821-sample tuning set determined an optimal learning rate of 0.03 and 300 trees (Figure S3). The final model was then trained using the combined 90% of samples (7387 samples, achieving a final training-sample-to-feature ratio of 56.8:1) and evaluated against the remaining independent 10% (820 samples) alongside field measurements. A ratio exceeding 50:1 is generally robust for gradient boosting trees; combined with proper hyperparameter tuning and RFE, this configuration controls model complexity.

Validation results showed that for the Jiagedaqi District, the GBT model achieved an R^2 of 0.58, an MAE of 0.72 m, and an RMSE of 1.01 m (Figure 10).

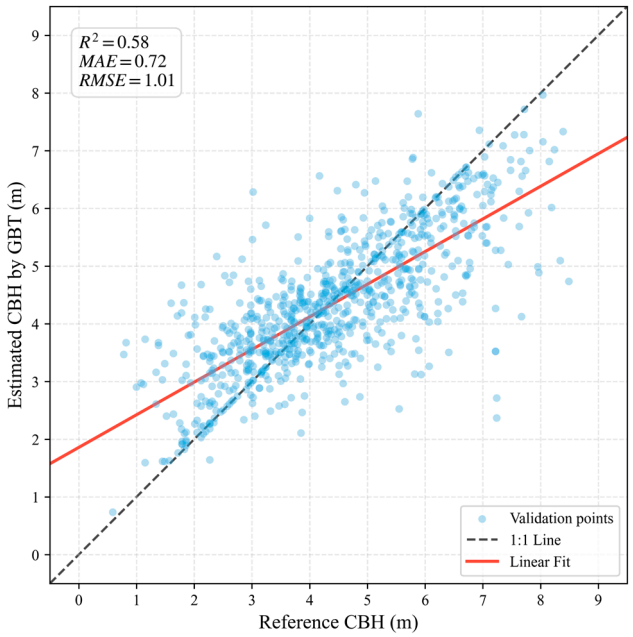


Figure 10. Validation of canopy base height (CBH) extrapolation using the gradient boosting tree (GBT) model against reference data derived from independent GEDI and ground measurements. The dashed black line represents the 1:1 reference, and the solid red line denotes the linear regression fit.

The contribution of each feature to the model is shown in Figure 11. The July and August mean values of Sentinel-2 Band 11 (SWIR; central wavelength = 1.610 μm) emerged as the most important predictors, contributing substantially more than other variables. This prominence can be attributed to the strong sensitivity of SWIR reflectance to canopy water content, woody biomass, and shadowing effects, which are closely linked to vertical canopy structure and the position of the crown base. During mid-summer, when foliage is fully developed and moisture conditions are relatively stable, SWIR signals are particularly effective in distinguishing crown and trunk structural characteristics relevant to CBH.

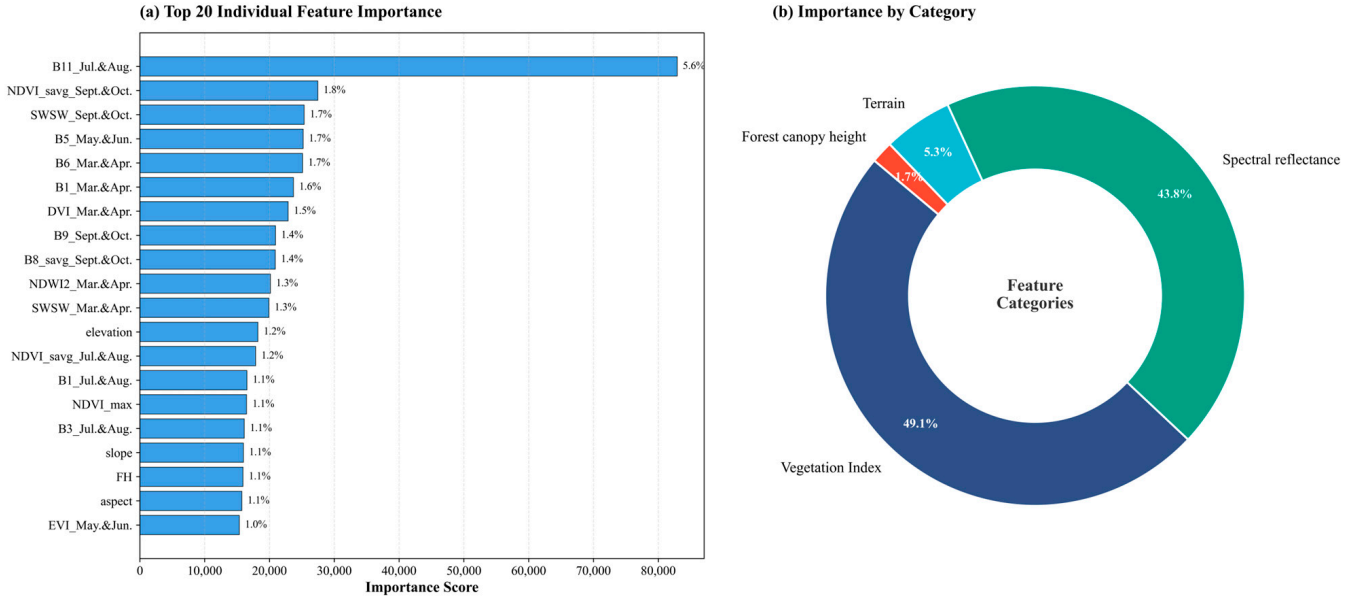


Figure 11. Relative contribution of different feature categories and individual predictors to the GBT model for CBH estimation. The highest contribution was from the July and August mean values of Sentinel-2 Band 11 (SWIR, central wavelength = 1.610 μm).

In terms of feature categories, vegetation indices accounted for the largest contribution (49.12%), followed by spectral features (43.83%), while topographic variables (5.35%) and forest canopy height (1.70%) played comparatively minor roles. The dominance of vegetation indices and spectral bands highlights the importance of canopy biochemical and structural information captured by optical remote sensing for CBH prediction. In contrast, topography and canopy height provide more indirect or coarse structural constraints, which contribute less to explaining the variability of CBH once detailed spectral information is available.

3.4. Spatial Distribution of CBH

The final trained GBT model was applied to produce wall-to-wall CBH maps for the Jiagedaqi District. As shown in Figure 12, CBH values exhibit a clear spatial gradient, with generally higher values in the western part of the region and lower values in the east. The enlarged sub-regions (Figure 12b–d), together with the corresponding Sentinel-2 imagery (Figure 12e–g), indicate that the spatial patterns of the estimated CBH are consistent with observed canopy conditions.

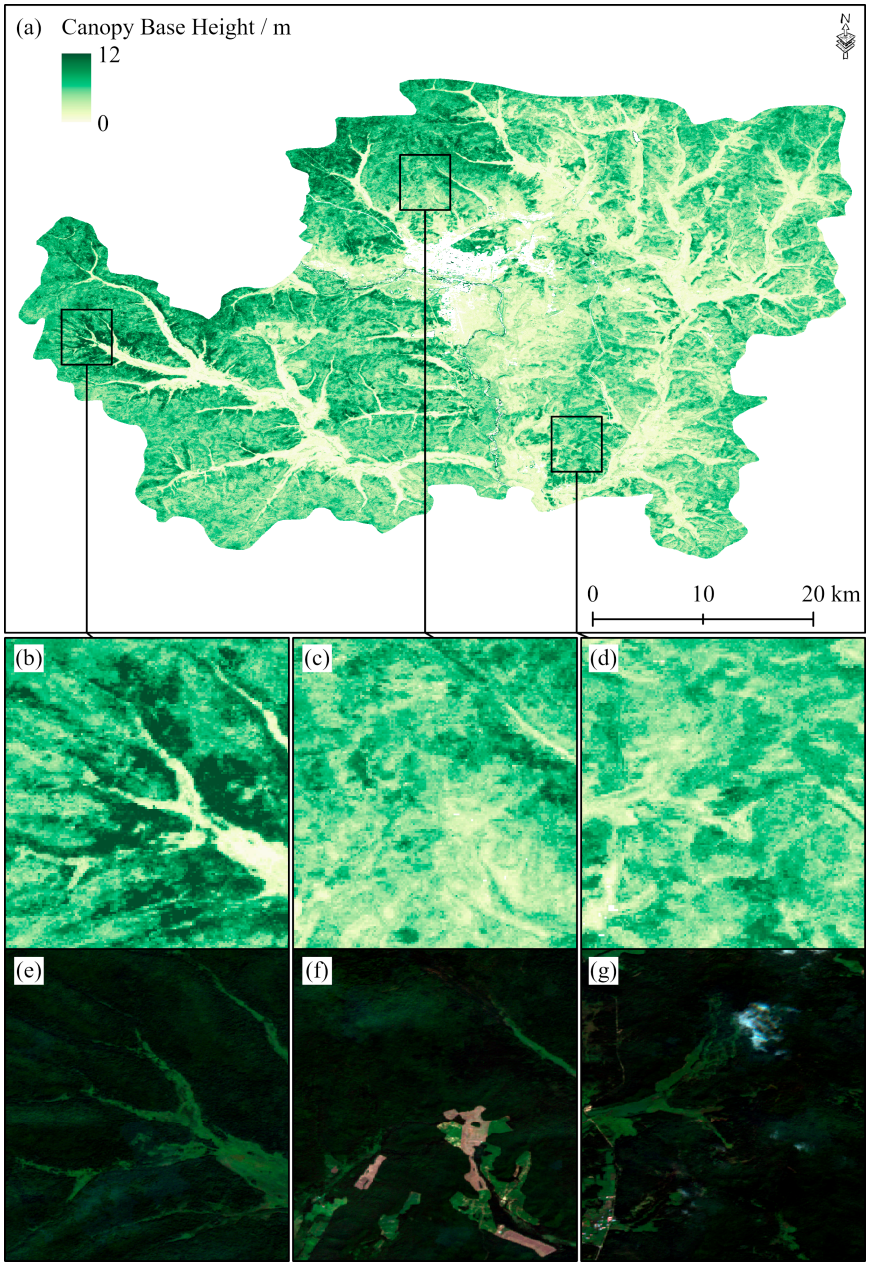


Figure 12. Spatial distribution of canopy base height in the Jiagedaqi District. (**a**) Full CBH map; (**b**,**d**,**f**) enlarged sub-regions; (**c**,**e**,**g**) corresponding Sentinel-2 imagery for the sub-regions.

4. Discussion

4.1. Reinterpreting Canopy Base Height from GEDI RH Profiles

Canopy base height has traditionally been treated as a discrete height variable to be predicted through empirical relationships with remote sensing metrics [30,31]. However, this perspective does not fully reflect the structural nature of CBH, which represents the transition between ground–understory elements and the lower boundary of the live canopy rather than a sharply defined geometric surface. Our results demonstrate that GEDI waveform-derived RH profiles inherently encode this vertical transition and can therefore be used to infer CBH as a structural breakpoint embedded within the cumulative energy distribution, rather than as an externally calibrated height target.

By interpreting the full RH vector (RH0–RH100) as a continuous representation of vertical vegetation–laser interactions, this study moves beyond percentile-based proxies and reframes CBH retrieval as a problem of identifying changes in vertical structural

continuity. The consistency between GEDI-derived CBH estimates and independent UAV LiDAR observations supports the physical validity of this interpretation and highlights the capacity of spaceborne waveform LiDAR to resolve canopy structural boundaries under suitable conditions.

This conceptual shift—from predicting CBH as a regression output to detecting it as a structural transition—provides a more physically grounded basis for CBH estimation and helps explain why CBH has remained more difficult to retrieve than canopy height or canopy cover in previous GEDI-based studies.

4.2. Advantages of Full-Profile Interpretation over Percentile-Based CBH Estimation

Most existing GEDI-based CBH studies rely on a limited subset of RH percentiles or empirically selected waveform metrics, implicitly assuming that CBH can be approximated by a single height indicator [1,23]. While such approaches have demonstrated feasibility at large scales, they consistently report substantially lower accuracy for CBH compared to canopy height, reflecting the intrinsic ambiguity of CBH as a structural parameter.

Our comparison of multiple RH-profile-based approaches shows that methods explicitly exploiting the entire vertical distribution of waveform energy are better suited to capture the crown–ground transition. In particular, the clustering-threshold approach demonstrated greater robustness across structurally heterogeneous stands, suggesting that CBH detection benefits from identifying changes in vertical energy density rather than relying on fixed percentile thresholds. This finding aligns with the physical interpretation of CBH as a transition zone characterized by a shift in vegetation density, rather than a single reflective surface.

Importantly, the proposed framework reduces the reliance of the GEDI-based CBH retrieval on allometric equations, forest inventory data, and region-specific airborne LiDAR calibration, which are commonly used in previous studies to compensate for the limited interpretability of individual RH metrics [1,2,30]. By directly interpreting GEDI height profiles, the method provides an operational pathway for CBH mapping that is less dependent on region-specific calibration and more closely tied to the underlying measurement physics. UAV LiDAR is used in this study only for independent validation and threshold sensitivity assessment, not for calibrating the GEDI-derived CBH itself.

It is worth noting that, because the clustering boundary is defined statistically as the local minimum in energy density between the ground and canopy modes, it represents an intermediate transitional position rather than the exact height of the lowest continuous live foliage. In stands with short trunks and deep, dense crowns, the large volume of upper foliage shifts the canopy energy mode upward, which can elevate the resulting statistical threshold and lead to a slight upward bias in the retrieved CBH. This effect is a deliberate consequence of relying on a robust statistical transition that effectively suppresses noise from understory and mid-story returns within the 25 m GEDI footprint, and the overall agreement with UAV LiDAR observations indicates that the retrieved CBH remains physically meaningful.

4.3. Structural Conditions Governing the Reliability of GEDI-Based CBH Retrieval

The reliability of GEDI-derived CBH estimates is fundamentally constrained by forest vertical structure. Our quality filtering strategy revealed that CBH can be robustly detected only when the waveform energy profile exhibits a clear two-layer structure, characterized by a distinct separation between ground returns and canopy returns. Under these conditions, the crown–ground transition manifests as a recognizable structural breakpoint within the RH profile.

In contrast, footprints associated with dense understory vegetation, multi-layered canopies, or vertically continuous foliage distributions often lack a discernible transition zone. As illustrated in Figure S4, such cases exhibit a smooth and continuous RH distribution in which the boundary between ground and canopy cannot be unambiguously resolved. Independent UAV LiDAR observations and field photographs confirm that these filtered-out footprints correspond to structurally complex stands where CBH itself becomes difficult to define even with high-resolution three-dimensional data.

Rather than representing methodological failure, these excluded cases highlight the physical limits of waveform-based CBH retrieval. When vertical vegetation density changes gradually rather than abruptly, CBH ceases to be a well-defined structural attribute. The applied filtering strategy therefore reflects a deliberate trade-off between sample quantity and structural interpretability, prioritizing physically meaningful CBH estimates over maximum footprint utilization (Table S1). This distinction is critical for large-scale applications, as it emphasizes that CBH retrievability depends not only on algorithm design but also on intrinsic forest structure.

The detectability of CBH using waveform LiDAR is fundamentally constrained by phenological conditions and canopy density. To formalize the physical limitations of the strict two-layer assumption, we conducted a sensitivity analysis linking algorithm performance to canopy cover. A logistic regression model revealed that successful structural transition detection requires a minimum canopy cover threshold of approximately 0.89 to maintain a >50% success probability (Figure S5). In such high-cover scenarios, the dense upper canopy effectively absorbs laser energy and obscures mid-story noise, creating the idealized physical boundary. Consequently, the 47% data retention rate is not an algorithmic artifact but a strict physical constraint; the framework intentionally discards complex, low-density waveforms to prioritize high-confidence structural estimations.

Furthermore, temporal tracking of identical forest footprints quantified the uncertainty introduced by seasonal foliage variations. Throughout the active growing season, the structural transition algorithm maintained robust detection capabilities. For instance, phenological shifts between early summer and early autumn altered the penetration depth of the waveform marginally, introducing a minor uncertainty of approximately ± 0.3 m (e.g., fluctuating between 5.2 m and 5.8 m) in CBH estimation (Figure S6). Conversely, under complete leaf-off conditions in winter, the lack of foliage resulted in waveform collapse, and the algorithm physically rejected the observations. Therefore, while the framework ensures stable CBH retrieval with sub-meter uncertainty during the growing season, its application must be temporally restricted to leaf-on periods to avoid false structural interpretations from bare branches.

4.4. Implications for Large-Scale CBH Mapping and Fire-Related Applications

The ability to retrieve CBH directly from GEDI RH profiles has important implications for large-scale forest structure monitoring. CBH is a key variable in canopy fuel characterization and fire behavior modeling, yet it is rarely available as a spatially continuous product due to its measurement difficulty [2]. By demonstrating that CBH can be inferred from spaceborne LiDAR without requiring region-specific airborne LiDAR calibration of the GEDI-based CBH retrieval—with airborne or UAV LiDAR used only for independent validation—this study expands the potential utility of GEDI for fire-related applications, habitat assessment, and ecosystem modeling.

Integration with Sentinel-2 imagery enables the spatial extrapolation of GEDI-derived CBH samples, providing wall-to-wall coverage while preserving the physical interpretability of waveform-based structural information. Although the present analysis focuses on a single study region, the methodological framework is transferable and can be applied

to other forest systems where canopy–ground transitions are structurally resolvable. To illustrate this potential cross-biome transferability, we conducted an independent proof-of-concept test in a complex subtropical mixed forest (Xichang, Southwestern China). Unlike the boreal stands in our primary study area, this region features substantially different crown architectures (e.g., broadleaf *Juglans regia* mixed with coniferous species) and a dense understory shrub layer. As illustrated in Figure S7, despite the considerable structural interference, the adaptive multi-cluster framework was able to decouple the continuous understory from the main canopy. The algorithm identified the energy transition point at 4.49 m, which closely aligned with the canopy gap fraction observed in the corresponding UAV LiDAR profile slice. This single-plot test provides preliminary evidence that the detection framework is not solely tailored to boreal stands and that it can respond to vertical vegetation density patterns in structurally different biomes; further multi-site validation will be required to confirm its broader transferability. At broader scales, such an approach could support regional assessments of canopy fuel continuity and improve the representation of vertical forest structure in Earth system models.

4.5. Limitations and Future Research Directions

Several limitations should be acknowledged. First, while CBH itself is a relatively stable structural attribute, its detectability using GEDI waveform data is influenced by phenological conditions in deciduous forests. Leaf-off conditions reduce canopy return energy and weaken vertical stratification, limiting the identification of crown-base transitions (Figure S6). This seasonal sensitivity reflects constraints of the observation system rather than changes in CBH and should be considered when designing large-scale applications. Beyond this phenological constraint, two additional limitations warrant detailed discussion. The first concerns the reliance on optical proxies for regional extrapolation, which introduces signal saturation in dense canopies and motivates the supplementary integration of Synthetic Aperture Radar (SAR) data. The second concerns the strict two-layer structural assumption underlying the GEDI waveform clustering, which restricts footprint retention in complex multi-layered stands and motivates the development of an adaptive multi-cluster algorithm. Each of these limitations and the corresponding methodological considerations are examined in turn below.

4.5.1. Optical Saturation and Multi-Source Fusion

In our feature importance analysis, both topographic variables (5.35%) and forest canopy height (FH) (1.70%) showed comparatively minor contributions relative to spectral proxies such as SWIR Band 11. This pattern can be attributed to two interacting factors. First, the Jiagedaqi District is characterized by gently undulating low hills with an average elevation of 472 m. Under this relatively homogeneous topography, topographic variables do not induce the pronounced microclimatic or structural gradients typically observed in mountainous alpine regions. Second, while FH defines the uppermost canopy boundary, CBH is primarily driven by stand density, light competition, and natural self-pruning. Trees of similar heights can therefore exhibit different CBHs depending on local canopy closure. Because the Sentinel-2 SWIR bands are sensitive to canopy shadowing, leaf moisture, and woody biomass, they indirectly but effectively capture the local foliage density and canopy closure that govern CBH, which makes the broader constraints of topography and canopy height largely redundant in the decision tree splits.

However, this reliance on optical proxies introduces a critical limitation in dense forests. The high dispersion observed in the GBT model at extreme (particularly high) CBH values is directly linked to the saturation of optical signals, such as Sentinel-2 Band 11. High CBH typically occurs in mature, closed-canopy stands with high Leaf Area Indices

(LAIs). In these environments, the dense upper foliage saturates the shortwave infrared signals, rendering the model insensitive to deeper sub-canopy structural variations.

To mitigate this dispersion and partially overcome optical signal saturation, the integration of Synthetic Aperture Radar (SAR) data offers a useful complementary source of information. To explore this, we conducted a supplementary analysis incorporating bi-seasonal Sentinel-1 C-band features (leaf-on vs. leaf-off). Despite the substantial data gap over our region during 2022 (due to the Sentinel-1B anomaly), we utilized 2021 SAR data, assuming short-term structural stability of the woody framework.

The inclusion of these microwave features yielded insightful improvements. Notably, the feature importance analysis revealed that the seasonal difference in cross-polarization backscatter emerged as a significant predictor. This parameter effectively captures the seasonal attenuation of the radar signal through the leaf layer, serving as a direct physical proxy for canopy density. Consequently, the model's overall predictive capability improved, with R^2 rising from 0.58 to 0.61.

Interestingly, while the overall explained variance (R^2) improved, the RMSE remained stable (1.01 m) and the MAE saw a marginal increase (from 0.72 m to 0.77 m). This statistical trade-off highlights the physical nature of C-band SAR: it effectively corrects severe structural saturation at extreme CBH values in dense stands (thereby boosting R^2) but introduces inherent microwave speckle noise to the broader distribution, slightly elevating the baseline absolute error.

While the temporal mismatch prevents these features from being integrated into our primary operational map, this supplementary evidence suggests that fusing GEDI-derived structural breakpoints with multi-temporal SAR (particularly cross-polarized volumetric scattering) and optical data is a promising strategy. As active microwave constellations are replenished, this multi-source fusion approach may become increasingly important for mitigating saturation limits and improving wall-to-wall CBH mapping in complex, multi-layered forests.

Beyond this optical–microwave fusion strategy, which primarily addresses signal saturation in the regional extrapolation stage, a second structural limitation arises at the footprint-scale retrieval stage itself: the strict two-layer waveform assumption underlying the GEDI clustering framework. This assumption restricts the algorithm's applicability in vertically complex stands and motivates the adaptive multi-cluster extension examined next.

4.5.2. Adaptive Multi-Cluster for Complex Stands

A further limitation arises from the framework's reliance on a clear vertical separation between canopy and ground layers. Future work could explore methods capable of resolving CBH under more complex vertical structures, potentially through advanced waveform decomposition, multi-peak analysis, or integration with complementary spaceborne LiDAR observations such as ICESat-2. To address this constraint within the present study, we evaluated an adaptive multi-cluster extension of our framework, as detailed below.

While the strict "two-layer" structural assumption ensures high purity of the extracted CBH samples (RMSE = 1.27 m), it also leads to the exclusion of a large proportion of GEDI footprints characterized by complex vertical structures (resulting in a retention rate of 47.14% for the clustering-threshold method). This trade-off between physical interpretability and sample quantity raises a relevant question: is this profile-based detection framework viable in complex ecosystems where multi-layered structures are prevalent, such as tropical rainforests or dense mixed forests?

To evaluate the framework's potential and efficiency in such complex stands, we developed and tested an "adaptive multi-cluster" algorithm. When a waveform is parti-

tioned into more than two clusters due to the presence of dense understory or multi-layered canopies, this algorithm redefines the physical boundary of the CBH as the energy transition point between the "ground class" and the "lowest vegetation class."

Adopting this adaptive multi-cluster strategy substantially increased the effective footprint retention rate to 81.37%. As shown in Figure S8, validation against independent UAV LiDAR data further indicated that the model's accuracy remained stable in these complex structures (R^2 = 0.69, RMSE = 1.41 m, and MAE = 1.09 m). Compared to the strictly filtered "two-layer" samples, the inclusion of multi-layered stands introduced only a modest increase in error.

This finding has practical operational implications. It suggests that deriving structural boundaries directly from GEDI RH profiles is not strictly limited to single-layer forests. For regional machine learning-based mapping that requires high-fidelity training data, conservative filtering remains a reasonable and valid trade-off. However, for broad-scale applications seeking to maximize spatial footprint utilization in complex ecosystems—such as assessing canopy fuel continuity across diverse biomes—the adaptive multi-cluster approach offers a viable alternative within the same physical filtering framework.

Despite these limitations, the results demonstrate that GEDI height profiles contain sufficient structural information to support physically meaningful CBH retrieval. By advancing the interpretation of spaceborne waveform LiDAR from percentile-based metrics toward structural transition detection, this study contributes to improved representation of forest vertical attributes and enhances the role of GEDI data in large-scale forest structure monitoring.

Therefore, the adaptive strategy is presented here as an extension for maximizing footprint utilization in structurally complex forests, whereas the conservative two-layer subset was retained for the primary wall-to-wall mapping to ensure high-confidence training labels.

5. Conclusions

This study developed a physically interpretable framework for estimating canopy base height by integrating spaceborne GEDI waveform LiDAR and Sentinel-2 optical data. By interpreting the full GEDI RH profile as a continuous representation of vertical vegetation structure, canopy base height was identified as a structural transition rather than approximated using predefined height percentiles. Evaluation against independent UAV LiDAR observations demonstrated that the clustering-threshold approach provides the most consistent agreement among the tested methods, supporting the feasibility of directly deriving CBH from GEDI height metrics. Sparse GEDI-derived CBH samples were further extrapolated to spatially continuous maps using a gradient boosting regression model and multisource optical predictors, capturing clear regional-scale patterns in canopy base height. Overall, this study advances the use of spaceborne waveform LiDAR for detecting forest structural boundaries and demonstrates the potential of GEDI data for large-scale mapping of fire-relevant canopy structure attributes.

Supplementary Materials: The following supporting information can be downloaded at https://www.mdpi.com/article/10.3390/rs18132092/s1, Figure S1: Dominant tree species observed in the field survey; Figure S2: Sensitivity analysis of the UAV point cloud stratification threshold; Figure S3: Recursive feature elimination results and hyperparameter optimization for the Gradient Boosting Tree (GBT) model; Figure S4: Example of a GEDI footprint excluded due to complex vertical forest structure; Figure S5: Sensitivity of Structural Transition Detection to Canopy Cover; Figure S6: Seasonal Dynamics of GEDI Relative Height Profiles; Figure S7: Cross-biome subtropical demonstration of the structural transition concept in a complex subtropical forest (Xichang, Southwestern China);

Figure S8: Comparison of canopy base height (CBH) estimation accuracy under different clustering constraints; Table S1: Footprint retention rates for different GEDI-based CBH estimation methods.

Author Contributions: L.Z.: Conceptualization, Formal analysis, Investigation, Methodology, Software, Validation, Visualization, Writing—original draft, Writing—review and editing. W.G.: Writing—review and editing. C.J.: Investigation, Funding acquisition, Writing—review and editing. All authors have read and agreed to the published version of the manuscript.

Funding: This work was supported by the Beijing Municipal Science and Technology Program Project (Z251100003625008), the National Key Research and Development Program of China (2020YFC1511602-01) and the Innovation and Development Union Project of Chongqing Natural Science Foundation (CSTB2025NSCQ-LZX0095).

Data Availability Statement: Data will be made available on request.

Conflicts of Interest: The authors declare no conflicts of interest.

References

1. Aragoneses, E.; Garcia, M.; Ruiz-Benito, P.; Chuvieco, E. Mapping forest canopy fuel parameters at European scale using spaceborne LiDAR and satellite data. *Remote Sens. Environ.* **2024**, *303*, 114005. [CrossRef]
2. Yang, Z.; Qi, Z.; Chen, Y.; Cheng, K.; Yang, H.; Chen, M.; Xu, J.; Zhang, Y.; Ren, Y.; Liu, W.; et al. Revealing the spatial distribution of crown base height across China based on close-range Lidar data. *Remote Sens. Environ.* **2025**, *331*, 115030. [CrossRef]
3. Andersen, H.-E.; McGaughey, R.J.; Reutebuch, S.E. Estimating forest canopy fuel parameters using LIDAR data. *Remote Sens. Environ.* **2005**, *94*, 441–449. [CrossRef]
4. Abdollahi, A.; Yebra, M. Challenges and Opportunities in Remote Sensing-Based Fuel Load Estimation for Wildfire Behavior and Management: A Comprehensive Review. *Remote Sens.* **2025**, *17*, 415. [CrossRef]
5. Guo, H.; Kong, L.; Gao, Y.; Xiang, D.; Li, Z.; Gong, L.; Zhang, Y. Transition from surface fire to crown fire and effects of crown height, moisture content and tree flower. *Fire Technol.* **2024**, *60*, 1403–1419. [CrossRef]
6. Noonan-Wright, E.K.; Opperman, T.S.; Finney, M.A.; Zimmerman, G.T.; Seli, R.C.; Elenz, L.M.; Calkin, D.E.; Fiedler, J.R. Developing the US wildland fire decision support system. *J. Combust.* **2011**, *2011*, 168473. [CrossRef]
7. Arellano-Pérez, S.; Castedo-Dorado, F.; López-Sánchez, C.A.; González-Ferreiro, E.; Yang, Z.; Díaz-Varela, R.A.; Álvarez-González, J.G.; Vega, J.A.; Ruiz-González, A.D. Potential of Sentinel-2A Data to Model Surface and Canopy Fuel Characteristics in Relation to Crown Fire Hazard. *Remote Sens.* **2018**, *10*, 1645. [CrossRef]
8. Kelly, M.; Su, Y.; Di Tommaso, S.; Fry, D.L.; Collins, B.M.; Stephens, S.L.; Guo, Q. Impact of Error in Lidar-Derived Canopy Height and Canopy Base Height on Modeled Wildfire Behavior in the Sierra Nevada, California, USA. *Remote Sens.* **2018**, *10*, 10.
9. Luo, L.; Zhai, Q.; Su, Y.; Ma, Q.; Kelly, M.; Guo, Q. Simple method for direct crown base height estimation of individual conifer trees using airborne LiDAR data. *Opt. Express* **2018**, *26*, A562–A578. [CrossRef] [PubMed]
10. Engelstad, P.S.; Falkowski, M.; Wolter, P.; Poznanovic, A.; Johnson, P. Estimating Canopy Fuel Attributes from Low-Density LiDAR. *Fire* **2019**, *2*, 38. [CrossRef]
11. Chamberlain, C.P.; Sánchez Meador, A.J.; Thode, A.E. Airborne lidar provides reliable estimates of canopy base height and canopy bulk density in southwestern ponderosa pine forests. *For. Ecol. Manag.* **2021**, *481*, 118695. [CrossRef]
12. Wang, Y.; Xi, X.; Wang, C.; Yang, X.; Wang, P.; Nie, S.; Du, M. A Novel Method Based on Kernel Density for Estimating Crown Base Height Using UAV-Borne LiDAR Data. *IEEE Geosci. Remote Sens. Lett.* **2022**, *19*, 1–5. [CrossRef]
13. Popescu, S.C.; Zhao, K. A voxel-based lidar method for estimating crown base height for deciduous and pine trees. *Remote Sens. Environ.* **2008**, *112*, 767–781. [CrossRef]
14. Yueliang, G.; Ge, G.; Li, X.; Ji, C.; Wang, T.; Shen, T.; Zhi, Y.; Chen, C.; Zhao, L. The Aboveground Biomass Estimation of the Grain for Green Program Stands Using UAV-LiDAR and Sentinel-2 Data. *Sensors* **2025**, *25*, 2707. [CrossRef] [PubMed]
15. Bu, J.; Xiao, J. Upscaling eddy covariance measurements of carbon and water fluxes to the continental scale by incorporating GEDI-derived canopy structural complexity metrics. *Remote Sens. Environ.* **2025**, *329*, 114930. [CrossRef]
16. Dubayah, R.; Blair, J.B.; Goetz, S.; Fatoyinbo, L.; Hansen, M.; Healey, S.; Hofton, M.; Hurtt, G.; Kellner, J.; Luthcke, S.; et al. The Global Ecosystem Dynamics Investigation: High-resolution laser ranging of the Earth's forests and topography. *Sci. Remote Sens.* **2020**, *1*, 100002. [CrossRef]
17. Ahmad, A.; Sastry, S.; Dhakal, A.; Khanal, S.; Levering, A.; Gilani, H.; Jacobs, N. Canopy height mapping in the Western Himalayas, Pakistan: A deep learning approach using GEDI and Sentinel-2 fusion. *Int. J. Appl. Earth Obs. Geoinf.* **2026**, *146*, 105030. [CrossRef]

18. Potapov, P.; Li, X.; Hernandez-Serna, A.; Tyukavina, A.; Hansen, M.C.; Kommareddy, A.; Pickens, A.; Turubanova, S.; Tang, H.; Silva, C.E.; et al. Mapping global forest canopy height through integration of GEDI and Landsat data. *Remote Sens. Environ.* **2021**, *253*, 112165. [CrossRef]
19. Lang, N.; Jetz, W.; Schindler, K.; Wegner, J.D. A high-resolution canopy height model of the Earth. *Nat. Ecol. Evol.* **2023**, *7*, 1778–1789. [CrossRef] [PubMed]
20. Duncanson, L.; Kellner, J.R.; Armston, J.; Dubayah, R.; Minor, D.M.; Hancock, S.; Healey, S.P.; Patterson, P.L.; Saarela, S.; Marselis, S.; et al. Aboveground biomass density models for NASA's Global Ecosystem Dynamics Investigation (GEDI) lidar mission. *Remote Sens. Environ.* **2022**, *270*, 112845. [CrossRef]
21. Shendryk, Y. Fusing GEDI with earth observation data for large area aboveground biomass mapping. *Int. J. Appl. Earth Obs. Geoinf.* **2022**, *115*, 103108. [CrossRef]
22. Schneider, F.D.; Ferraz, A.; Hancock, S.; Duncanson, L.I.; Dubayah, R.O.; Pavlick, R.P.; Schimel, D.S. Towards mapping the diversity of canopy structure from space with GEDI. *Environ. Res. Lett.* **2020**, *15*, 115006. [CrossRef]
23. Heisig, J.; Milenković, M.; Pebesma, E. High-resolution canopy fuel maps based on GEDI: A foundation for wildfire modeling in Germany. *Environ. Res. Ecol.* **2025**, *4*, 015003. [CrossRef]
24. Zhao, L.; Shi, Y.; Liu, B.; Hovis, C.; Duan, Y.; Shi, Z. Finer Classification of Crops by Fusing UAV Images and Sentinel-2A Data. *Remote Sens.* **2019**, *11*, 3012. [CrossRef]
25. Zhao, L.; Ji, C.; Ge, G.; Shen, T.; Yang, H.; Xiao, T.; Wang, T.; Yueliang, G.; Li, X. Neglecting non-photosynthetic vegetation leads to serious underestimation of the wind erosion prevention service provided by the Grain for Green Program in Inner Mongolia, China. *Int. J. Digit. Earth* **2025**, *18*, 2543566. [CrossRef]
26. Zhang, X.; Liu, L.; Chen, X.; Gao, Y.; Xie, S.; Mi, J. GLC_FCS30: Global land-cover product with fine classification system at 30 m using time-series Landsat imagery. *Earth Syst. Sci. Data* **2021**, *13*, 2753–2776. [CrossRef]
27. NASA JPL. *NASA Shuttle Radar Topography Mission Global 1 Arc Second [Data Set]*; NASA EOSDIS Land Processes Distributed Active Archive Center (LP DAAC): Sioux Falls, SD, USA, 2013. [CrossRef]
28. Zhao, L.; Guo, W.; Wang, J.; Wang, H.; Duan, Y.; Wang, C.; Wu, W.; Shi, Y. An Efficient Method for Estimating Wheat Heading Dates Using UAV Images. *Remote Sens.* **2021**, *13*, 3067. [CrossRef]
29. Haralick, R.M.; Shanmugam, K.; Dinstein, I.H. Textural features for image classification. *IEEE Trans. Syst. Man Cybern.* **1973**, *SMC–3*, 610–621. [CrossRef]
30. Ex, S.A.; Smith, F.W.; Keyser, T.L.; Rebain, S.A. Estimating Canopy Bulk Density and Canopy Base Height for Interior Western US Conifer Stands. *For. Sci.* **2016**, *62*, 690–697. [CrossRef]
31. Arkin, J.; Coops, N.C.; Daniels, L.D.; Plowright, A. Canopy and surface fuel estimations using RPAS and ground-based point clouds. *For. Int. J. For. Res.* **2023**, *98*, 15–28. [CrossRef]

Disclaimer/Publisher's Note: The statements, opinions and data contained in all publications are solely those of the individual author(s) and contributor(s) and not of MDPI and/or the editor(s). MDPI and/or the editor(s) disclaim responsibility for any injury to people or property resulting from any ideas, methods, instructions or products referred to in the content.